To appear in Ap. J.

On the Relation Between Peak Luminosity and Parent Population of Type Ia Supernovae: A New Tool for Probing the Ages of Distant Galaxies

Valentin D. Ivanov, Mario Hamuy, Philip A. Pinto

Steward Observatory, The University of Arizona, Tucson, AZ 85721,
vdivanov, mhamuy, & ppinto@as.arizona.edu

ABSTRACT

We study the properties of Type Ia Supernovae (SNe Ia) as functions of the radial distance from their host galaxy centers. Using a sample of 62 SNe Ia with reliable luminosity, reddening, and decline rate determinations, we find no significant radial gradients of SNe Ia peak absolute magnitudes or decline rates in elliptical+S0 galaxies, suggesting that the diversity of SN properties is not related to the metallicity of their progenitors. We do find that the range in brightness and light curve width of supernovae in spiral galaxies extends to brighter, broader values. These results are interpreted as support for an age, but not metallicity, related origin of the diversity in SNe Ia. If confirmed with a larger and more accurate sample of data, the age-luminosity relation would offer a new and powerful tool to probe the ages and age gradients of stellar populations in galaxies at redshift as high as $z \sim 1-2$. The absence of significant radial gradients in the peak $(B-V)_0$ and $(V-I)_0$ colors of SNe Ia supports the redding correction method of Phillips *et al.* (1999). We find no radial gradient in residuals from the SN Ia luminosity-width relation, suggesting that the relation is not affected by properties of the progenitor populations and supporting the reliability of cosmological results based upon the use of SNe Ia as distance indicators.

Subject headings: cosmology: observations – distance scale – galaxies: general – supernovae: general

1. Introduction

In recent years the search for a precise extragalactic distance indicator has stimulated the study of Type Ia Supernovae (hereafter SN Ia). A number of surveys (*e.g.* Hamuy et al. 1993, 1996a,b,c; Riess et al. 1999; Perlmutter et al. 1999) have yielded samples with high-quality light curves and well-defined selection criteria. The availability of such data provides an opportunity for studying SNe Ia at an unprecedented level of detail.

Perhaps the most important result of these surveys is that the SNe Ia do not constitute a homogeneous family of objects – SNe Ia are not all the same. They span a range in peak B luminosity of approximately three magnitudes and exhibit a variety of light curve morphologies (Maza et al. 1994; Hamuy et al. 1995). Their heterogeneity has also been demonstrated spectroscopically (Phillips et al. 1992).

While the discovery of a significant dispersion in peak brightness seemed to spell disaster for the use of SNe Ia as extragalactic standard candles, Phillips (1993) demonstrated a tight correlation between the peak luminosity and the rate of decline from peak in the first 15 days. This relation was refined by Hamuy et al. (1995), and shown to reduce the dispersion about the Hubble relation by a factor of two by Hamuy et al. (1996b). This dispersion was then reduced even further by Phillips et al. (1999), who included a precise correction for extinction to achieve a dispersion between 0.09 and 0.12 magnitudes, depending on photometric band.

Riess, Press, & Kirshner (1996), using a different statistical technique, have also shown that the light curve shape near peak is an accurate predictor of luminosity. Perlmutter et al. (1997) have demonstrated that not only is there a correlation of the light curve shape with luminosity but that, near peak, the light curve is the *same* in all supernovae up to a correlated scaling in time and luminosity. All three methods are capable of achieving similarly accurate determinations of a supernova's peak brightness.

The discovery and refinement of the luminosity-width relation in SNe Ia has enabled Riess et al. (1999) and Perlmutter et al. (1999) to use observations of SNe Ia over a large range of redshifts to show that the cosmological expansion is accelerating at a rate which cannot be explained without the introduction of new physics such as a cosmological constant.

It is widely accepted that SNe Ia result from the thermonuclear incineration of a carbon/oxygen white dwarf, and that the light curve is powered by the radioactive decay of ^{56}Ni produced in the explosion. The systematic diversity of SNe Ia may provide important clues to the nature of their progenitors and the explosion mechanism. It has been suggested that the range in peak luminosities displayed by SNe Ia reflects a range in the nucleosynthetic ^{56}Ni yield. Höflich & Khokhlov (1996) demonstrated that a variety of light curve shapes could be generated from various explosion models, and that the width of the light curve was correlated in some models with the ^{56}Ni mass. Pinto & Eastman (2000) showed that changing only the ^{56}Ni yield in a typical explosion model can reproduce both the slope and the absolute normalization of the luminosity-width relation to well within the observed dispersion. Neither of these models explains the origin of SN Ia diversity, however.

Unfortunately, much of the most important physics in current models for the evolution and explosion of SNe Ia is far too complex to be modeled in anything close to a predictive fashion. For example, because we lack a detailed theory of turbulent combustion, the behavior of the nuclear burning rate, critical to the properties of the resulting explosion, must be put in "by hand". Höflich, Wheeler, & Thielemann (1998), and Umeda et al. (1999a,b) have explored the effects of progenitor age and metallicity on SN properties using one particular set of assumptions. They find that in this

case the supernova progenitor's properties affect the ^{56}Ni production and the light curve width, with younger and more metal-rich progenitors leading to brighter SNe Ia.

An additional route towards understanding the origin of SN Ia diversity is the study of the supernova environments, in particular the location of the supernovæ in the host galaxy. Since properties of the stellar population differ from galaxy to galaxy and vary with location within a galaxy, such studies can show which properties of the parent population affect the nature of the SN Ia explosion.

Hamuy et al. (1996a) found that faster-declining (fainter) SNe Ia tend to occur in earlier-type galaxies, suggesting that the age of the progenitor is a significant parameter. This result was confirmed by Riess et al. (1999), who also found that after correcting peak absolute magnitudes for extinction and applying the width-luminosity relation, there was no residual difference in the corrected supernova magnitudes between early- and late-type galaxies.

The location of SNe in their host galaxies has been extensively studied (*cf.* van den Berg 1997 and references therein). Shaw (1979) noted a deficiency of SNe Ia in the innermost regions of galaxies, but attributed it to a selection effect; in photographic surveys, it is difficult to discern SNe against the higher background on which they are projected near the centers of the galaxies. Wang, Höflich, & Wheeler (1997) and Howell, Wang, & Wheeler (2000) later confirmed this effect, at least in the older photographic SNe searches. Hamuy & Pinto (1999) also showed this to be the case in a more rigorous analysis of the Calán-Tololo survey.

Major problems which have plagued these and similar studies of the radial gradients of SNe Ia in their host galaxies include the difficulty of determining true galactocentric distances and the intrinsic spread of properties among the host galaxies themselves. The goal of this paper is to use the best-observed sample of SNe Ia available to study the radial distribution of SNe Ia in their host galaxies and the variations of their properties with galactocentric distance. We improve on these previous studies by: (i) deprojecting the observed angular distances between the SN and the host galaxy center, removing ambiguities arising from projecting the distances on the plane of the sky; (ii) normalizing such distances to the sizes of the hosts; (iii) applying statistical methods to estimate the significance of radial gradients in SN properties; and (iv) exploring the possible applications of SNe Ia as tools to probe the stellar populations of distant galaxies. We will compare our results with current theoretical understanding of the origin of the peak luminosity - decline rate relation, and will assess consistency with the known radial variation of age and metallicity in galaxies.

2. The SNe Ia Sample: Selection and Properties

Our sample consists of 62 well-observed SNe Ia (listed in Table 1) with reliable estimates of peak luminosity, reddening, and decline rate $\Delta m_{15}(B)$ as determined by Phillips et al. (1999); throughout this paper we use only the reddening-corrected absolute magnitudes as presented in that work. Several SNe with no peak BVI measurements were used exclusively in tests that require

only positional information. SN1992K and SN1991bg were excluded from our analysis as peculiarly subluminous; there is considerable debate in the supernova community as to whether these objects are a different sort of explosion or merely the faintest tail of the "normal" supernovae distribution.

The Hubble type and redshifts of the host galaxies were taken from the NASA/IPAC Extragalactic Database (hereafter NED). The galaxy semi-major axes and position angles are taken from the RC3 (de Vaucouleurs et al. 1999), the UGC (Nilson 1973), and the ESO/Upsala catalogs (Holmberg et al. 1974). For galaxies with no available measurements in the literature, we determined galaxy parameters from the Calán/Tololo B-band images. SN peak magnitudes and decline rates were determined by template-fitting following the prescription of Hamuy et al. (1996a). We use Cepheid distances measured by Gibson et al. (2000) for six nearby SNe, and distance derived from observed redshifts for the remainder of the sample. Throughout this paper we adopt a value for the Hubble constant $H_0 = 69$ km sec^{-1} Mpc^{-1} for consistency with the Gibson *et al.* distances. We also assume a cosmology with $\Omega_0 = 0.2$, $\Omega_\Lambda = 0.0$ to calculate the linear galactocentric distances.

To de-project the angular distances of SNe Ia from the centers of disk galaxies, we assume that all SNe Ia populate disks which are thin compared with the galaxy diameters. This is a reasonable assumption for spirals and, perhaps, for S0 galaxies. To compute actual galactocentric distances, we express the SN position in a radial coordinate system centered at the host galaxy nucleus and aligned with the semi-major axis. We then use the axial ratio to calculate the inclination of the disk. In most cases the projected angular offsets (listed in Table 1) come from the discovery announcements of the supernovae, with positions verified against the NED. We did not de-project the angular distances for the SNe in ellipticals as the depths of these galaxies along the line of sight are comparable to their apparent sizes.

The distributions of the major properties of our sample are shown in Figure 1. 23 SNe are in elliptical and S0 hosts and 39 in spirals. Observational selection (Hamuy & Pinto 1999) accounts for the higher redshift of the SNe in elliptical+S0 than in spirals; early-type galaxies tend to dominate the statistics for larger projected galactocentric distances. Reddening in spirals is seen to be higher than in early-type galaxies, with the notable exception of SN1986G ($E(B-V) = 0.50 \pm 0.05$ mag) whose host is the peculiar S0 Seyfert 2 galaxy NGC 5128. Naturally, we find in our sample a deficiency of SNe fainter than $M_B = -19$ mag, with $E(B-V) > 0.10$ mag.

The brightness at maximum light of SNe Ia in our sample is related to the morphological type of the host galaxy. Hamuy et al. (1996a) pointed out that faster-declining (fainter) SNe tend to occur in earlier type galaxies, a result later confirmed by Riess et al. (1999). We carried out a Kolmogorov-Smirnov (hereafter KS) test between the peak absolute magnitude distributions for the SNe in early-type and late-type galaxies. The significance level P for the null hypothesis that the two sets of data are drawn from the same parent distribution is given in Table 2. Small values of P suggest that the distributions are different. We obtained only 2, 2 and 7% of probability, that the distributions of SNe Ia peak magnitudes, respectively for B, V, and I-band observations, in elliptical+S0 galaxies and spirals were drawn from the same parent distribution. The higher

probability for the I-band reflects the smaller amplitude of the luminosity-width relation in the near infrared. The rate of decline is an even better indicator of a difference between SNe Ia in early- and in late-type galaxies, giving a significance level of only 0.001%. The de-reddened $(B-V)_0$ SNe colors, on the other hand, are identical to a confidence level of 90%. The very small uncertainties in this analysis reflect major differences of the intrinsic properties of the host galaxies such as age, metallicity, and dust content, and strongly suggest that the properties of SNe Ia are determined by their environments.

3. Radial Gradients of SNe Ia Properties

The SN host galaxies show a spread of sizes, masses and metallicities – presumably because larger and more massive galaxies can better retain the heavy elements produced by stellar evolution (Arimoto & Yoshii 1987). Galaxy-to-galaxy abundance variations can be corrected, to some extent, by a proper normalization of galactocentric distances. Following van den Berg (1997), we divided the galactocentric distances by the semi-major axis. This approach has the advantage that the semi-major axis can be used as a "metalometer". Since semi-major axes are not always accurately known, we will carry out our analyses using both normalized and absolute radial distances, for comparison.

We first carried out linear fits for the absolute peak magnitude against the linear distance R_{dp} (in Kpc) and for the distance normalized to the semi-major axis R_{dp}/a. We then calculated the residuals Δ from the luminosity-width relation for each SN, using the quadratic form of the relation given by Phillips et al. (1999), in order to look for trends of Δ with galactocentric distance. We then computed fits for the decline rate Δm_{15} against both distances. Table 3 lists the coefficients, their 1σ errors in brackets, and the standard deviation of the fits shown in Figure 2. We carried out separate analyses for the entire sample, for SNe in elliptical+S0 galaxies, and for SNe in spirals. We concentrate on fits to B-band magnitudes and widths because the amplitude of the luminosity-width rate relation is the largest at these wavelengths, rendering our results both more sensitive to differences among supernovae and to the de-reddening procedure employed by Phillips *et al.*.

Taking into account the entire sample, we find that SNe closer to the galaxy centers are brighter, in agreement with the conclusion of Wang, Höflich, & Wheeler (1997). However, when we divide the SNe Ia according to the host galaxy type, we find no significant radial gradient of the absolute peak magnitudes. The gradient in the sample as a whole can easily be understood; a brighter population of SNe Ia in spirals dominates the sample at small galactocentric distances ($R_{dp} \leq 7.5$) while the fainter population of SNe Ia in ellipticals and S0's dominates at larger radial distances ($R_{dp} > 7.5$).

There seems to be a small but significant $(2-5\sigma)$ correlation between decline rate and radial distance, but this result is due mainly to one object (SN1992bo) illustrating the importance of extending the SN sample. When the early- and late-type galaxies are treated separately, the

decline rate gradient is reduced by a factor of 2 or more. Employing normalized radial distances makes the trends of Δm_{15} with distance disappear at the $2 - 2.5\sigma$ level.

The de-reddened SNe Ia $(B-V)_0$ color at maximum light shows no radial variation (Figure 3). If we use the linear distance fits, the color change is only 0.03 mag over 30 Kpc for the entire sample. The change is just sightly larger for spirals alone (0.06 mag over 10 Kpc). Similarly, there is no radial gradient of $(V-I)_0$ color at peak within the uncertainties. This results lend credence to the reddening correction method of Phillips *et al.*.

4. Discussion

The radial metallicity gradient in elliptical galaxies is an established observational fact (Henry & Worthey 1999 and references therein; Kobayashi & Arimoto 1999; Tamura et al. 2000). At the same time, the population in these galaxies is co-eval (Worthey 1994; Vazdekis et al. 1996, 1997). The stars near the center of spiral galaxies are, however, in general both more metal rich *and* older when compared with outer regions (Henry & Worthey 1999; Bell & de Jong 2000). This difference provides an ideal opportunity to separate the effects of age and metallicity on SNe Ia properties.

The lack of any radial gradients in SNe Ia properties in elliptical+S0 galaxies suggests that neither the absolute peak magnitude nor the decline rate is a strong function of the metal abundance of the progenitor. The residuals from the luminosity-width relation seem also to be independent of metallicity in the host population. At the same time, SNe Ia in late-type galaxies exhibit a significantly different distribution in both peak magnitude and decline rate from their cousins in early-type galaxies.

These results are consistent with the hypothesis that the *age* of the progenitor, but not the metallicity, may be responsible for the diversity of SNe Ia peak luminosities and decline rates. Current theoretical understanding of the problem is fraught with uncertainties, but a possible scenario was suggested by Umeda et al. (1999a,b). They argue that, no matter what the details of explosive burning may be, the larger specific energy available from burning larger mass fractions of carbon in a C/O dwarf will result in greater ^{56}Ni production and, hence, brighter SNe Ia. They then argue that the oldest SN progenitor systems are those with the smallest-mass companions, and that these systems can transfer less mass in all to the pre-SN white dwarf. Thus, the pre-SN systems which take longest to evolve to explosion must be those with the largest initial C/O white dwarf mass. Since larger C/O core masses have smaller carbon abundances, these older systems will lead to lower ^{56}Ni masses, and eventually, fainter supernovae.

Such a scenario naturally explains the absence of bright SNe Ia in ellipticals, with their older populations, and is also consistent with the larger dispersion of peak luminosity found near the center of spiral galaxies (Wang, Höflich, & Wheeler 1997) where SNe Ia would be produced from a mixture of stellar populations with various ages.

Our results are consistent with the predictions of von Hippel et al. (1997) who carried out a semi-empirical modeling of the white dwarf mass function, and derived the SN Ia luminosity function for a range of progenitor masses and ages. Their work used the older sub-Chandrasekhar explosion models of Woosley & Weaver (1994), different from the Chandrasekhar mass explosions considered by Umeda et al. (1999a,b).

The range in accretion rate necessary to produce SNe Ia from Chandrasekhar white dwarfs in single-degenerate systems is quite narrow (Nomoto & Kondo 1991), too narrow to lead to a SNe Ia rate in accord with observations. Hachisu, Kato, & Nomoto (1996, 1999) have suggested that in systems with greater mass transfer rates, a wind may remove all but the necessary amount from the system, leading to a much broader range in binary systems capable of leading to SNe Ia. The wind is driven by radiation pressure on metal lines, and its strength thus depends upon both the metallicity of the system and the luminosity from burning accreted material. This luminosity is larger for larger C/O dwarf masses, and thus for a given C/O dwarf mass the metallicity of the system must be greater than some minimum value. Below a critical metallicity, the radiation momentum absorbed by the wind is insufficient to reduce the mass transfer rate below that leading to a common-envelope system. The papers by Umeda *et al.* suggest that this will lead to a metallicity effect on the range of SN Ia luminosities – the larger the C/O dwarf mass, the lower the critical metallicity required for the wind. Thus, lower-metallicity systems will tend to have larger initial C/O dwarf masses and hence fainter supernovæ.

This metallicity effect seems not to be supported by our results. Since we do not find strong radial variation of the SNe Ia parameters separately in elliptical+S0 galaxies, and in spirals, such an effect seems unlikely to explain the lack of bright supernovae in the ellipticals. Indeed, as we find no variation in supernova properties with radius in early-type galaxies, any wind in SN Ia progenitor systems must be much less sensitive to metallicity than posited by Hachisu, Kato, & Nomoto.

Given a range in ^{56}Ni yield, Pinto & Eastman (2000) show that this is in itself sufficient to lead to the observed luminosity-width relation. They suggest that this relation is thus unlikely to be affected by metallicity effects on the radiation transport responsible for the relation, and the lack of any radial gradient in SN properties in ellipticals and S0's bears this out.

Most of the SNe Ia with Cepheid calibrations (Gibson et al. 2000) happen to lie at large radial distances in their host galaxies and are therefore fainter than average. One might be concerned that a selection bias against SNe Ia at small angular separations from their host galaxy centers (the "Shaw effect") would make local and distant samples of SNe Ia incommensurate. Our results imply that after correcting for extinction and luminosity-width relation, SNe Ia become true standard candles, independently of their galactocentric distance, and thus, metal abundance.

Indeed, the lack of any correlation found to the *corrected* supernovae magnitudes should be heartening to those employing SNe Ia at large redshifts to measure cosmological properties. The range in both metallicity and age spanned by the galaxies in our sample exceeds the difference in

average values of these parameters between the local universe and at a redshift $z \sim 1$. To explain away the cosmological results found by Riess et al. (1998) and by Perlmutter et al. (1999), the corrected peak magnitudes of the lower metallicity and/or younger supernovae found at $z \sim 1$ would have to be fainter on average by more than 0.2 mag, a result clearly ruled out by Figure (2).

At lesser distances, the lack of any gradient in residuals from the luminosity-width relation argues against a bias in the determination of the Hubble constant based on intrinsically fainter nearby SNe Ia.

A possible test of the relation between the peak luminosities (and light curve shapes) of SNe Ia and the age of their progenitor populations can be carried via spectral indices age diagnostics of the host galaxy population (Worthey 1994; Vazdekis et al. 1996, 1997). If confirmed, this relation might be used to probe the ages and age gradients of stellar populations in galaxies. The intrinsic brightness of these SNe makes it possible to carry out such an analysis to redshifts beyond $z \sim 1$ with current observational capabilities. Such a technique is rendered even more important by the advent of new telescopes and instruments in the near future. For instance, Dahlén & Fransson (1999) estimate that NGST is expected to detect about 45 SNe Ia per field in a single 10^4 sec exposure, with mean redshift of z $\approx$ 2. From the ground, the 8.4m wide-field Dark Matter Telescope proposed by Hinz,Wolf, & Angel (1999) would provide high-quality observations of many hundreds of supernovae per year to $z \sim 1.5$ (Pinto 1999, private communication).

5. Summary

Our KS tests confirm the result of Hamuy et al. (1996a) that SNe Ia in elliptical+S0 and in spiral host galaxies are intrinsically different, with faster-declining (fainter) SNe Ia occurring mostly in earlier-type galaxies.

We find no significant radial variation of the SNe Ia peak absolute brightness in ellipticals+S0s and in spirals. Taken together, SNe do show a correlation in peak brightness with radial distance. This is a consequence of the fact that fainter SNe Ia are found in ellipticals, and these SNe dominate the sample at larger galactocentric distances.

Our analysis shows no significant radial gradient of the reddening-corrected peak magnitude $(B-V)_0$ and $(V-I)_0$ colors, lending support to the reddening correction method of Phillips et al. (1999).

The peak absolute luminosity and the decline rate of SNe Ia are independent of the metallicity of the SNe progenitors, within the observational uncertainties. Determinations of extragalactic distances and related cosmological parameters are thus not biased by metallicity- or age-related evolutionary effects.

Our results are consistent with an age-related origin of the luminosity-width relation. If confirmed, this age *vs.* decline rate relation in SNe Ia offers an important new tool to probe the ages

and age gradients of stellar populations in galaxies at redshifts as high as $z \sim 1 - 2$.

We are grateful to Dr. M.M. Phillips for the useful discussions. The research has made use of the NASA/IPAC Extragalactic Database which is operated by the Jet Propulsion Laboratory, California Institute of Technology, under contract with NASA. This work has been supported by the National Science Foundation (CAREER grant AST9501634). PAP gratefully acknowledges support from the Research Corporation though a Cottrell Scholarship.

Table 1. Data for the supernovae sample.

SN 19xx	Host Galaxy Name	Hubble Type	T Type	Redshift z^{helio}	a × b arcmin	P.A. deg	M_B/σ mag	M_V/σ mag	M_I/σ mag	$E(B-V)/\sigma$ mag	$\Delta m_{15}/\sigma$ mag	R_p arcsec	R_{dp} arcsec
90O	MCG+03-44-003	SBa	1	0.030664	0.80x0.80	125	-19.46/21	-19.43/19	-18.97/18	0.02/03	0.96/10	27	27
90T	PGC63925	SA(s)00	0	0.040400	1.30x0.70	85	-19.52/28	-19.45/23	-19.06/20	0.09/04	1.15/10	19	20
90Y	FCCB1147	E(M32?)	-5	0.039200	0.46x0.46	0	-19.42/28	-19.51/23	-18.96/20	0.23/04	1.13/10	5	5
90af	[TB93]2131.14-6257.7	SB0	0	0.050300	0.47x0.42	0	-19.08/16	-19.07/13	-	0.04/03	1.56/05	0	0
91S	UGC05691	Sb	3	0.055000	1.10x0.80	140	-19.47/27	-19.42/21	-19.01/19	0.06/04	1.04/10	18	24
91U	IC4232	Sbc:pec	4	0.031442	1.10x0.30	2	-19.80/29	-19.75/24	-19.43/21	0.11/04	1.06/10	3	6
91ag	IC4919	SB(s)dmPec	8	0.014223	1.50x0.70	31	-19.75/36	-19.71/36	-19.29/37	0.07/03	0.87/10	21	27
92J	[M92b]100643-2624.0	S	5	0.045000	1.00x0.70	85	-18.95/28	-19.04/22	-18.72/19	0.03/04	1.56/10	18	23
92K	ESO269-G057	(RS)SAB(r)b	3	0.010274	3.20x2.30	54	-17.53/47	-18.29/44	-18.44/43	0.00/04	1.93/10	14	19
92P	IC3690	Sb:	3	0.025401	1.10x0.30	6	-19.51/21	-19.41/19	-19.03/18	0.07/03	0.87/10	10	17
92ae	[WM92]212426.8-614612	E1?	-5	0.070000	1.10x0.90	0	-19.53/20	-19.49/15	-	0.12/04	1.28/10	5	5
92ag	ESO508-G067	S?	5	0.025164	1.00x0.20	101	-19.42/25	-19.42/22	-19.10/19	0.10/04	1.19/10	6	12
92al	ESO234-G069	SAB(s)c	5	0.014600	2.10x0.70	111	-19.52/33	-19.43/32	-19.08/32	0.01/03	1.11/05	23	39
92aq	[HM92]230149-3736.8	Sa?	1	0.101000	0.26x0.21	0	-18.81/19	-18.90/14	-18.46/12	0.00/04	1.46/10	6	6
92au	[HM92a]000808-5013.6	E1	-5	0.062000	0.31x0.26	0	-18.97/27	-19.00/21	-18.53/18	0.00/04	1.49/10	23	23
92bc	ESO300-G009	Sab	2	0.020160	1.20x0.40	44	-19.60/24	-19.50/23	-19.14/23	0.00/02	0.87/05	5	9
92bg	[MH92d]074119.0-622406	Sa	1	0.035000	0.76x0.29	40	-19.36/20	-19.30/17	-18.95/15	0.01/03	1.15/10	6	8
92bh	[MH92e]045840.0-585410	Sbc	4	0.044000	0.63x0.37	135	-19.35/17	-19.29/14	-18.91/12	0.12/03	1.05/10	3	4
92bk	ESO156-G008	S0-pec	0	0.059007	0.77x0.45	0	-19.00/17	-18.98/13	-18.75/11	0.01/03	1.57/10	70	81
92bl	ESO291-G011	(R1)SB(s)0/a	0	0.044000	1.10x0.80	108	-19.04/17	-19.03/15	-18.73/13	0.00/03	1.51/10	25	35
92bo	ESO352-G057	SB(s)00pec	0	0.018963	1.40x0.40	12	-18.74/27	-18.72/26	-18.57/25	0.00/03	1.69/05	74	144
92bp	[M92n]033422.3-183104	E2/S0	-5	0.080000	0.45x0.33	45	-19.39/14	-19.31/12	-18.95/10	0.00/03	1.32/10	6	6
92br	[MH93]014355.4-562057	E0	-5	0.088000	0.19x0.18	0	-18.68/24	-18.68/16	-	0.01/04	1.69/10	14	14
92bs	FCCB0602	Sc(s)II	5	0.064000	0.48x0.32	120	-19.30/19	-19.25/15	-	0.10/04	1.13/10	23	27
93B	[MH93a]103235.1-341103	SBb	3	0.069000	0.34x0.24	140	-19.42/17	-19.41/14	-18.96/12	0.12/03	1.04/10	5	6
93H	ESO445-G066	SB(r)ab	2	0.024247	1.10x1.00	0	-18.16/25	-18.43/22	-18.54/20	0.05/04	1.69/10	7	7
93O	[HM93]132819-3257.6	E5/S01	-5	0.051000	0.22x0.09	80	-19.18/16	-19.08/13	-18.81/11	0.00/03	1.22/05	14	14
93ag	[HM93a]100125-3513.1	E3/S01	-5	0.070000	0.40x0.24	110	-19.13/17	-19.12/14	-18.74/12	0.07/03	1.32/10	13	13
93ah	ESO471-G027	SBb(rs)	3	0.029494	1.00x0.40	2	-19.27/30	-19.20/25	-18.86/23	0.01/04	1.30/10	12	12
93ac	CGCG307-023	E	-5	0.049304	-	130	-19.36/23	-19.26/18	-19.06/13	0.12/04	1.19/10	35	35
93ae	UGC1071	E	-5	0.019049	1.40x1.20	0	-19.22/34	-19.15/30	-18.91/29	0.00/03	1.43/10	29	29
94M	NGC4493	E	-5	0.022955	0.86x0.67	148	-19.17/23	-19.12/21	-18.91/20	0.08/03	1.44/10	28	28
94Q	PGC059076	S0	0	0.028965	0.54x0.31	90	-19.41/31	-19.36/25	-18.98/23	0.06/04	1.03/10	4	6
94S	NGC4495	Sbc	4	0.015166	1.40x0.80	130	-19.46/30	-19.44/29	-19.10/28	0.00/03	1.10/10	16	24
94T	CGCG016-058	Sa	1	0.034664	-	55	-19.09/21	-19.09/18	-18.83/15	0.09/04	1.39/10	13	13
94ae	NGC3370	Sc	5	0.004265	3.20x1.80	148	-19.29/82	-19.26/81	-18.79/81	0.12/03	0.86/05	26	38
95D	NGC2962	S0	0	0.006545	2.60x1.90	3	-19.57/58	-19.49/57	-19.07/57	0.04/02	0.99/05	94	101
95E	NGC2441	Sb	3	0.011558	2.00x1.70	20	-19.86/40	-19.86/39	-19.53/38	0.74/03	1.06/05	22	26
95ac	P95cJ224541-0845.2	S	5	0.049990	-	55	-19.85/20	-19.78/16	-19.48/13	0.08/04	0.91/05	4	4
95ak	IC1844	Sbc	4	0.023008	0.70x0.25	105	-19.53/24	-19.43/22	-19.16/21	0.18/03	1.26/10	8	9
95al	NGC3021	SA(rs)bc:	4	0.005139	1.60x0.90	110	-19.37/74	-19.35/73	-18.86/73	0.15/03	0.83/05	17	23
95bd	UGC3151	S	5	0.015991	1.10x0.25	97	-19.57/43	-19.71/37	-19.32/31	0.15/06	0.84/05	23	26
96C	MCG+08-25-47	Sa	1	0.029572	1.00x0.50	10	-19.42/24	-19.39/22	-19.00/25	0.09/03	0.97/10	143	200
96X	NGC5061	E0	-5	0.006775	3.50x3.00	0	-19.68/57	-19.66/57	-19.37/56	0.01/02	1.25/05	60	60
96Z	NGC2935	Sb	3	0.007584	3.60x2.80	0	-19.89/54	-19.86/52	-32.88/50	0.33/04	1.22/10	69	70
96ai	NGC5005	SBcd	6	0.003169	5.80x2.80	65	-20.12/112	-20.42/112	-19.74/111	1.44/04	0.99/10	22	28
96bk	NGC5308	S0	0	0.006806	3.70x0.70	60	-18.24/71	-18.69/63	-18.59/62	0.19/05	1.75/10	24	34
96bl	[P96]J003618.17+112334	SBc	5	0.035965	-	0	-19.58/19	-19.55/17	-19.24/15	0.08/03	1.17/10	6	6
96bo	NGC673	Sc	5	0.017254	2.10x1.70	0	-19.56/30	-19.61/29	-19.21/28	0.28/03	1.25/05	6	8
96bv	UGC3432	Scd:	6	0.016706	1.70x0.40	136	-19.82/30	-19.75/28	-19.45/27	0.21/03	0.93/10	6	8

Table 1—Continued

SN 19xx	Host Galaxy Name	Hubble Type	T Type	Redshift z^{helio}	a × b arcmin	P.A. deg	M_B/σ mag	M_V/σ mag	M_I/σ mag	$E(B-V)/\sigma$ mag	$\Delta m_{15}/\sigma$ mag	R_p arcsec	R_{dp} arcsec
37C	IC4182	SA(s)m	9	0.001071	6.00x5.50	0	-19.74/17	-19.68/17	-	0.03/03	0.87/10	61	68
72E	NGC5253	ImpecHII	10	0.001348	5.00x1.90	45	-19.39/22	-19.33/21	-19.05/23	0.01/03	0.87/10	119	213
80N	NGC1316	(R)SAB(s)00LINER	0	0.005871	12.00x8.50	50	-	-	-	0.05/02	1.28/04	214	270
81B	NGC4536	SAB(rs)bcHII	4	0.006031	7.60x3.20	130	-19.45/15	-19.42/12	-	0.11/03	1.10/07	56	99
86G	NGC5128	S0pecSy2	0	0.001825	25.70x20.00	35	-	-	-	0.50/05	1.73/07	106	126
89B	NGC3627	SAB(s)bSy	3	0.002425	9.10x4.20	173	-19.26/24	-19.24/22	-19.04/20	0.34/04	1.31/07	51	59
90N	NGC4639	SAB(rs)bcSy1.8	4	0.003369	2.80x1.90	123	-19.52/16	-19.46/13	-19.07/11	0.09/03	1.07/05	62	77
91T	NGC4527	SAB(s)bcHII/LINER	4	0.005791	6.20x2.10	67	-	-	-	0.14/05	0.94/05	51	83
91bg	NGC4374	E1	-5	0.003336	6.50x5.60	135	-16.79/24	-17.51/17	-17.88/12	0.03/05	1.93/10	57	57
92A	NGC1380	SA0	0	0.006261	4.80x2.30	7	-18.50/14	-18.47/12	-18.18/11	0.00/02	1.47/05	62	71
94D	NGC4526	SA(s)b:sp	3	0.008427	4.50x0.80	113	-19.09/12	-19.03/11	-18.79/10	0.00/02	1.32/05	12	16
98bu	NGC3368	SAB(rs)abSy	2	0.002992	7.60x5.20	5	-19.47/16	-19.43/14	-19.18/13	0.33/03	1.01/05	55	55

Note. — Notation: z^{helio} - heliocentric redshift; a,b - semi-major and semi-minor axis, arcmin; P.A. - position angle, deg; M_B, M_V, M_I - reddening corrected SN absolute peak magnitudes in B, V and I-bands, respectively; E(B-V) - total SN reddening, as determined by Phillips et al. (1999); Δm_{15} - decline rate, mag; σ - 1σ observational error for the peak magnitudes, the reddening and decline rate, in hundredth of a magnitude; R_p - projected angular galactocentric distance, in arcsec; R_{dp} - deprojected galactocentric distance for spirals and S0s.

Table 2. Comparison between the parameters of the SNe in different types of host galaxies. The significance level P, % from the Kolmogorov-Smirnov test is given (see Section 2 for details).

Parameter	N_{Ell+S0}	N_{Spiral}	P,%
M_B	17	35	2
M_V	17	35	2
M_I	14	32	7
$(B-V)_0$	21	38	90
Δm_{15}	23	39	0.001
$E(B-V)$	23	39	12

Table 3. Fit coefficients to a linear relation Y=A+B*X for the radial gradients of the absolute magnitudes, residuals from the peak brightness vs. decline rate relation, and the colors of the SNe Ia from our sample.

X	Y	#	A	B	σ
All Types of Host Galaxies					
R_{dp}^{Kpc}	M_B	56	-19.419(0.044)	0.022(0.006)	0.350
R_{dp}^{Kpc}	Δ_B	56	-0.060(0.065)	0.004(0.008)	0.210
R_{dp}/a	M_B	52	-19.368(0.044)	0.245(0.087)	0.340
R_{dp}/a	Δ_B	52	-0.065(0.067)	0.100(0.129)	0.211
R_{dp}^{Kpc}	Δm_{15}	56	1.055(0.013)	0.021(0.002)	0.216
R_{dp}/a	Δm_{15}	52	1.094(0.014)	0.201(0.024)	0.235
R_{dp}^{Kpc}	$(B-V)_0$	56	-0.039(0.058)	0.001(0.007)	0.095
R_{dp}/a	$(B-V)_0$	52	-0.033(0.058)	-0.003(0.114)	0.097
R_{dp}^{Kpc}	$(V-I)_0$	50	-0.310(0.056)	0.003(0.007)	1.907
R_{dp}/a	$(V-I)_0$	46	-0.296(0.058)	-0.003(0.103)	1.989
Elliptical and S0 Host Galaxies					
R_{dp}^{Kpc}	M_B	20	-19.153(0.081)	0.006(0.008)	0.376
R_{dp}^{Kpc}	Δ_B	20	-0.010(0.121)	0.000(0.011)	0.209
R_{dp}/a	M_B	19	-19.138(0.074)	0.091(0.103)	0.379
R_{dp}/a	Δ_B	19	-0.053(0.114)	0.069(0.152)	0.214
R_{dp}^{Kpc}	Δm_{15}	20	1.279(0.024)	0.010(0.002)	0.211
R_{dp}/a	Δm_{15}	19	1.336(0.025)	0.058(0.029)	0.218
R_{dp}^{Kpc}	$(B-V)_0$	20	-0.029(0.106)	-0.001(0.010)	0.119
R_{dp}/a	$(B-V)_0$	19	-0.021(0.096)	-0.019(0.134)	0.120
R_{dp}^{Kpc}	$(V-I)_0$	17	-0.382(0.119)	0.007(0.010)	0.138
R_{dp}/a	$(V-I)_0$	16	-0.345(0.102)	0.043(0.130)	0.117
Spiral Host Galaxies					
R_{dp}^{Kpc}	M_B	36	-19.495(0.064)	0.022(0.015)	0.268
R_{dp}^{Kpc}	Δ_B	36	-0.113(0.098)	0.016(0.021)	0.212
R_{dp}/a	M_B	33	-19.411(0.073)	0.032(0.245)	0.274
R_{dp}/a	Δ_B	33	-0.085(0.103)	0.012(0.022)	0.214
R_{dp}^{Kpc}	Δm_{15}	36	1.003(0.020)	0.016(0.005)	0.182
R_{dp}/a	Δm_{15}	33	1.116(0.024)	-0.258(0.089)	0.187
R_{dp}^{Kpc}	$(B-V)_0$	36	-0.057(0.086)	0.006(0.019)	0.084
R_{dp}/a	$(B-V)_0$	33	-0.051(0.098)	0.057(0.327)	0.082
R_{dp}^{Kpc}	$(V-I)_0$	33	-0.303(0.081)	0.005(0.019)	2.357
R_{dp}/a	$(V-I)_0$	30	-0.268(0.094)	-0.061(0.316)	2.474

Note. — Notation: R_{dp}^{Kpc} - the projected galactocentric distance of the SN, Kpc; R_{dp}/a - the projected galactocentric distance of the SN normalized to the semi-major axis of the host galaxy; M_B - the reddening corrected absolute peak B-band magnitude of the SN; Δ_B - the residual from the SN absolute B-band peak luminosity vs. the decline rate relation, mag; σ - standard deviation, mag.

REFERENCES

Arimoto, N., & Yoshii, Y., 1987, A&A, 173, 23

Bell, E.F., & de Jong, R.S., 2000, MNRAS, 312, 497

Dahlén, T., & Fransson, C., 1999, A&A, 350, 349

de Vaucouleurs, G., de Vaucouleurs, A., Corwin, J.R., Buta, R.J., Paturel, G., & Fouque, P., 1991, Third Reference Catalog of Bright Galaxies, (Springer-Verlag Berlin Heidelberg New York).

Gibson, B.K., Stetson, P.B., Freedman, W.L., Mould, J.R., Kennicutt Jr., R.C., Huchra, J.P., Sakai, S., Graham, J.A., Fassett, C.I., Kelson, D.D., Ferrareze, L., Hughes, S.M.G., Illingworth, G.D., Macri, L.M., Madore, B.F., Sebo, K.M., & Silbermann, N.A., 2000, ApJ, 529, 723

Hachisu, I., Kato, M., & Nomoto, K. 1996, ApJ, 470, L97.

Hachisu, I., Kato, M., & Nomoto, K. 1999, submitted to ApJ.

Hamuy M., Maza, J, Phillips, M.M., Suntzeff, N.B., Wischnjewsky, M., Smith, R.C., Antezana, R., Wells, L., et al., 1993, AJ, 106, 2392

Hamuy M., Phillips, M.M., Maza, J., Suntzeff, N.B., Schommer, R.A., & Avilés, R., 1995, AJ, 109, 1

Hamuy M., Phillips, M.M., Schommer, R.A., Suntzeff, N.B., Maza, J., & Avilés, R., 1996b, AJ, 112, 2391

Hamuy M., Phillips, M.M., Maza, J., Suntzeff, N.B., Schommer, R.A., & Avilés, R., 1996a, AJ, 112, 2398

Hamuy M., Phillips, M.M., Suntzeff, N.B., Schommer, R.A., Maza, J., Antezana, R., Wischnjewsky, M., et al., 1996c, AJ, 112, 2408

Hamuy M., & Pinto, P.A., 1999, AJ, 117, 1185

Henry, R.B.C. & Worthey, G., 1999, PASP, 111, 919

Hinz, P., Wolf, N., & Angel, R., 1999, in "Working on the Fringe: An International Conference on Optical and IR Interferometry from Ground and Space", Dana Point, CA, May 24-27, 1999, ASP Conf. Ser. (Eds. S. Unwin and R. Stachnik), p. 55

Holmberg, E.B., Lauberts, A., Schuster, H.E., & West, R.M., 1974, A&AS, 18, 463

Howell, D.A., Wang, L., & Wheeler, J.C., 2000, ApJ, 530, 166

Höflich, P., & Khokhlov, A., 1996, ApJ, 472, L81

Höflich, P., Wheeler, J.C., & Thielemann, F.K., 1998, ApJ, 495, 617

Kobayashi, C., & Arimoto, N., 1999, ApJ, 527, 573

Maza, J., Hamuy, M., Phillips, M.M., Suntzeff, N.B., & Avilés, R., 1994, ApJ, 424, L107

Nilson, P., 1973, Nova Acta Regiae Soc. Sci. Upsaliensis, Ser. V:A, 1, 1

Nomoto, K. & Kondo, Y. 1991, ApJ, 367, 119.

Perlmutter, S. et al. 1997, ApJ, 483, 565

Perlmutter, S., Aldering, G., Goldhaber, G., Knop, R.A., Nugent, P., Castro, P.G., Deustus, S., Fabbro, S., et al., 1999, ApJ, 517, 565

Phillips, M.M., Wells, L.A., Suntzeff, N.B., Hamuy, M., Leibundgut, B., Kirshner, R.P., & Foltz, C.B., 1992, AJ, 103, 1632

Phillips, M.M., 1993, ApJ, 413, L105

Phillips, M.M., Lira, P., Suntzeff, N.B., Schommer, R.A., Hamuy, M., & Maza, J., 1999, AJ, 118, 1766

Pinto, P.A., & Eastman, R.G. 2000, submitted to ApJ

Riess, A.G., Press, W.H., & Kirshner, R.P., 1996, ApJ, 473, 88

Riess, A., et al. 1998, AJ, 116, 1009

Riess, A.G., Kirshner, R.P., Schmidt, B.P., et al., 1999, AJ, 117, 707

Shaw, R.L., 1979, A&A, 76, 188

Tamura, N., Kobayashi, C., Arimoto, N., Kodama, T., & Ohta, K., 2000, preprint (astro-ph/0001174)

Umeda, H., Nomoto, K., Yamaoka, H., & Wanajo, S., 1999a, AJ, 513, 861

Umeda, H., Nomoto, K., Kobayashi, C. Hachisu, I., & Kato, M., 1999b, ApJ, 522, L43

van den Berg, S., 1997, AJ, 113, 1

Vazdekis, A., Casuso E., Peletier, R.F., & Beckman, J.E., 1996, ApJS, 106, 307

Vazdekis, A., Peletier, R.F., Beckman, J.E., & Casuso E., 1997, ApJS, 111, 203

von Hippel, T., Bothun, G.D., & Schommer, R.A., 1997, AJ, 114, 115

Wang, L., Höflich, P., & Wheeler, J.C., 1997, ApJ, 483, L29

Woosley, S.E., & Weaver, T.A., 1994, ApJ, 423, 371

Worthey, G., 1994, ApJS, 95, 107

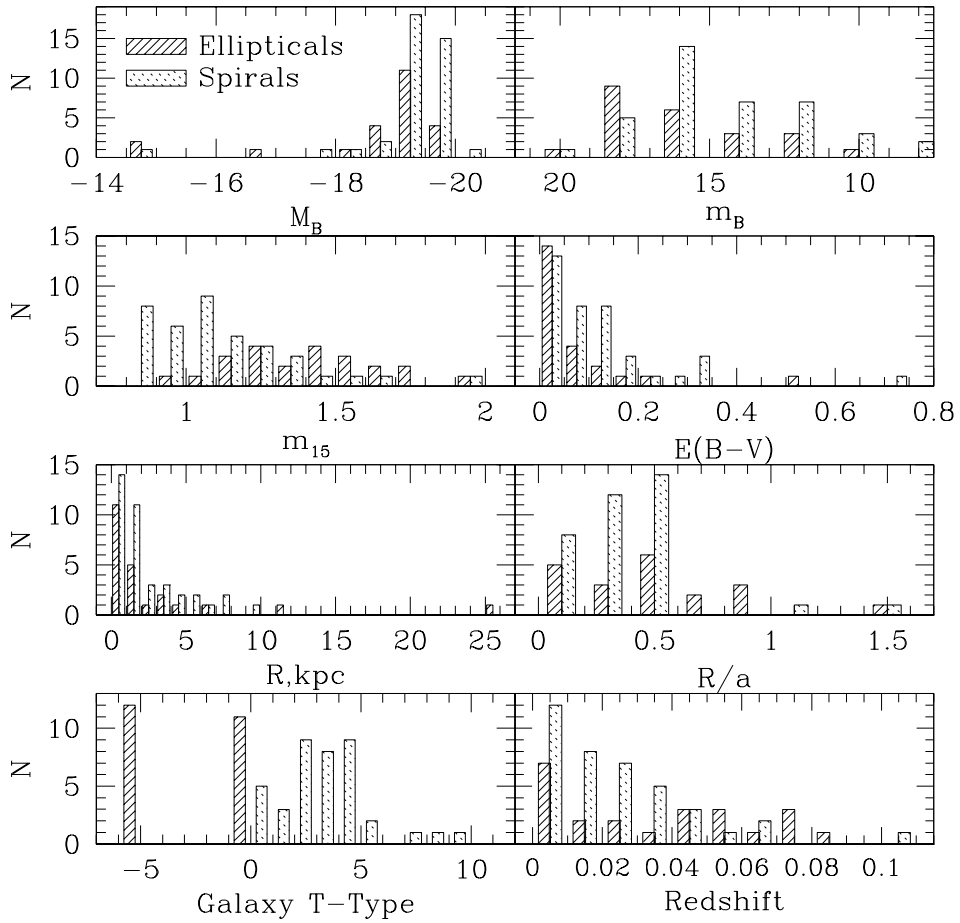

Fig. 1.— Properties of the SNe Ia sample. The distributions of SNe Ia in elliptical and S0 galaxies are given with solid lines, and the distributions of the SNe Ia in spirals are given with dashed lines.

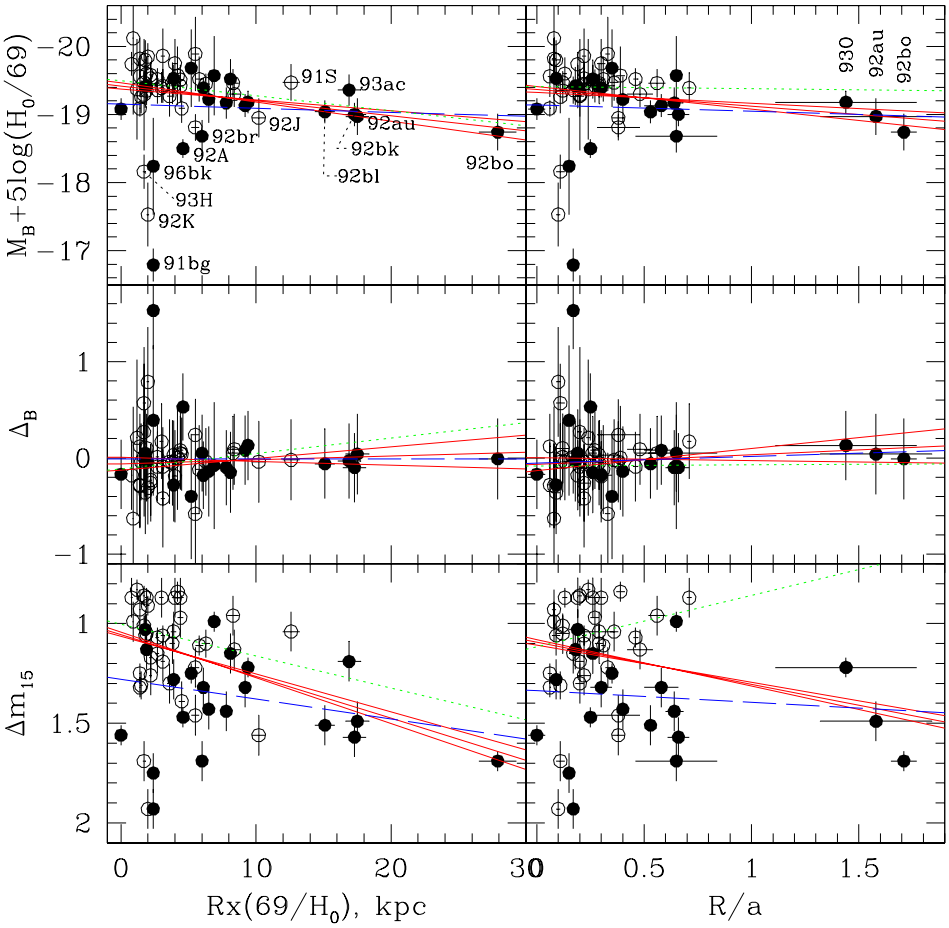

Fig. 2.— SN parameters as function of the galactocentric distances (left panels), and galactocentric distance normalized to the semi-major axis (right panels). The absolute B-band magnitude (M_B) is shown at the top. The residuals from the peak luminosity vs. decline rate relation (Δ_B) are shown at the center. The decline rate (Δm_{15}) is shown at the bottom. The open circles represent SNe Ia in spirals and the solid dots represent SNe Ia in elliptical and S0 galaxies. The fit to the entire sample and its 1σ errors are shown with solid lines, the fit to the SNe Ia in elliptical and S0 galaxies is shown with a dashed line and the fit to the SNe Ia in spirals is shown with a dotted line.

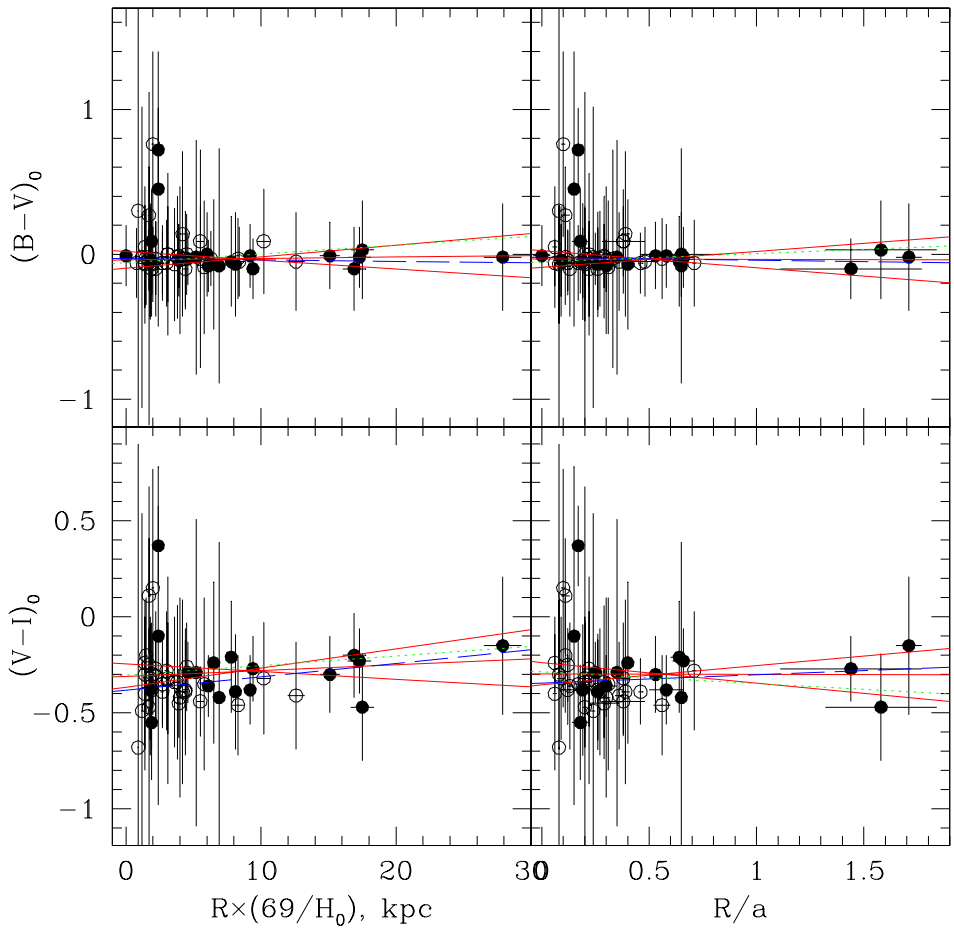

Fig. 3.— The reddening-corrected SN colors as function of the galactocentric distances (left panels), and galactocentric distance normalized to the semi-major axis (right panels). $(B-V)_0$ color is shown at the top panel, and $(V-I)_0$ color is shown at the bottom panel. The fits are indicated as in Figure 2.